https://doi.org/10.1016/j.matlet.2017.06.097

Structural, magnetic and transport properties of fully epitaxial $LaMnO_3/LaAlO_3$ multilayers

Y.K. Liu[1], H.F. Wong[1], S.Z. Huang[2], S.X. Hu[3], S.M. Ng[1], K.K. Lam[1], C.L. Mak[1] and C.W. Leung[1*]

[1]Department of Applied Physics, The Hong Kong Polytechnic University, Hong Kong, China

[2]Department of Physics, Southern University of Science and Technology, Shenzhen, China

[3]Materials Characterization and Preparation Center, Southern University of Science and Technology, Shenzhen, China

[*] Authors to whom correspondence should be addressed. Electronic mail: dennis.leung@polyu.edu.hk

Abstract

The structural, magnetic and transport properties of $LaMnO_3/LaAlO_3$(2 unit cells) (LMO/LAO) multilayers with different thicknesses of LMO layer grown on $SrTiO_3$ substrates were studied. Structural investigations confirmed that all the samples were fully epitaxial and the out-of-plane lattice constant increased with rising LMO layer thickness *t* from 1 to 4 unit cells. Ferromagnetic behavior could be observed only when *t* was above 2 unit cells, while the coercive field reduced with increasing *t*. Transport measurements indicated that all the multilayers were insulating and the activation energy of the multilayers were much larger than single-layered LMO films. These results provide a promising route for tuning the structure, electronic and magnetic properties in other strong-correlated materials.

Keywords: multilayer structure; epitaxial growth; magnetic properties ; manganites

Introduction

Heterostructures of transition-metal oxides (TMOs) have been a fertile ground for condensed matter physics and materials science, due to their fascinating properties and potential applications. These include colossal magnetoresistance in manganite, high-temperature superconductivity in cuprates, diluted magnetic semiconductors of doped zinc oxides, metal-insulator transition in nickel oxides [1-4]. These physical properties are closely related to the external stimuli: mechanical strain, carrier doping, and presence of fields (magnetic, electric and light), because of the complex interplay among the spin, charge, lattice and orbital degrees of freedom.

The prototypical perovskite TMO of $LaMnO_3$ (LMO) has received renewed interest recently for being an essential building block in various heterostructures that exhibit unexpected phenomena, such as exchange bias in LMO/$LaNiO_3$ multilayers [5], interface coupling in LMO/$SrTiO_3$ superlattices [6], ferromagnetism and metallic behavior at the interface of LMO/$SrMnO_3$ [7], orbital-order and possible superconductivity in $LaNiO_3$/LMO [8]. Here, we systematically investigate the structural variations of LMO/$LaAlO_3$ multilayers, and explore the magnetic and transport properties of the Mott insulator LMO bilayers sandwiched between 2 unit cells of wide band-gap insulator $LaAlO_3$ with varying LMO layer thickness.

Experimental details

A series of fully epitaxial multilayers of structure [$LaMnO_3$(t unit cells) /$LaAlO_3$(2 unit cells)]$_N$ (t = 1, 2, 3 and 4 unit cells) were grown on single crystal $SrTiO_3$ (STO) (001) substrates by pulsed laser deposition. STO crystals purchased from MTI Corp. were treated by a standard etching (in BHF solution) [9] and

annealing procedure at 1100˚C and 2h in oxygen, to realize a TiO_2-terminated surfaces. The stacking periodicity was repeated *N* times to adjust the total multilayer thickness to ~400 Å. The films were deposited at the substrate temperature of 720˚C and 26 Pa oxygen atmosphere, using a KrF excimer laser (λ = 248 nm) at 1 Hz with a laser fluence of 1.5 Jcm^{-2}. After deposition, the multilayers were annealed *in situ* at 1 atm oxygen atmosphere for 20 min to reduce the oxygen vacancies, and then cooled down naturally to room temperature.

Microstructure of the samples was characterized using an X-ray diffraction (SmartLab, Rigaku Co.) with a Cu K-α_1 radiation of wavelength λ_{XRD}=1.5406 Å. The magnetic and transport properties were measured using a Physical Property Measurement System (PPMS, Quantum Design Co.).

Results and discussions

Fig.1 shows the X-ray diffraction (XRD) θ-2θ scan patterns around (00*l*) peaks of $[(LMO)_t/(LAO)_2]_N$ multilayers. The obvious satellite peaks are indicative of the high crystallinity of the samples. Remarkably, the (00*l*) peaks shift towards lower angles with increasing *t*, which indicates an expansion of the *c*-axis lattice constant (*c*). The obtained lattice constants are c_1=3.77Å, c_2=3.80Å, c_3=3.82Å and c_4=3.83Å for *t* = 1, 2 3 and 4 unit cells (u.c.), respectively. The monotonic increment of *c*-axis lattice constant with increasing *t* is reasonable due to the larger lattice of LMO compared with LAO. All the multilayers have *c*-axis lattice constant much smaller than bulk of LMO, suggesting that all films are under tensile strain.

To further determine the microstructure of the samples, we performed reciprocal space mapping (RSM) measurements and the results are shown in Fig. 2. Only one major peak is observed for every multilayer in the RSM, and the multilayers and STO substrates possess the same in-plane lattice size, which

confirms the coherent and fully strained growth of the films. Due to this in-plane tensile strain, the out-of-lattice parameters are smaller than the bulk values, but shows larger values with increasing LMO layer thickness *t* as seen from the values of $Q_{\perp}$ (Fig. 2(a)-(d)) and is consistent with θ-2θ scan patterns (Fig.1). Thus, microstructural characterizations confirm the growth of spatially homogeneous and fully epitaxial high-quality $(LMO)_t/(LAO)_2$ multilayers.

Following the above structural evolutions, we investigated the variations of magnetic properties of the $[(LMO)_t/(LAO)_2]_N$ multilayers with different *t*. Ferromagnetic behavior was only observed when $t \geq 2$. Fig. 3(a) shows the normalized magnetization-temperature (*M*-*T*) curves of $[(LMO)_t/(LAO)_2]_N$ ($t \geq 2$) multilayers and the single layer LMO film grown on STO substrates, with both the measuring and cooling fields being 5000 Oe. For $t = 2$, the ferromagnetic transition temperature (T_C) of the sample is about 100 K [10], which is slightly smaller than bulk LMO film (~150 K) [11]. It is obvious that the T_C increases with thicker LMO, but is still smaller than the single-layer LMO film (Fig.3(a)). The magnetic hystereis curves of these multilayers at 5 K (Fig. 3(b)) exhibit very square loops with clear hysteresis centered at zero field. From Fig. 3(c) one can find that the coercive fields (H_C) of $[(LMO)_t/(LAO)_2]_N$ multilayers obtained from Fig. 3(b) reduces from 950 Oe for t=2 to 760 Oe for t=3 and then to 640 Oe for t=4 , but are still much larger than that of LMO film (295 Oe).

The origin of ferromagnetism in LMO film has been confirmed by a series of experiments [10-14] and theories [15-17], which arises intrinsically from strain-induced orbital ordering. From the structural characterization discussed above, the multilayers are under tensile strain, which is consistent with reported experiments [14] and theoretical calculations [15]. The enhancement of H_C may

be due to that non-magnetic LAO suppresses the interface magnetic coupling between the LMO layer, resulting in the weakened orbital ordering between LMO layers, leading to weaker FM behavior and larger coercive field［18］.

Fig. 4(a) shows the resistance of the samples as a function of temperature (*R*-*T*) for the multilayers and the bulk LMO film. As for sample with t = 1, the resistances of samples exceeded the measuring limit of our setup. From Fig. 4(a) one can see all the samples are highly insulating, and the *R*-*T* curves of LMO film (above 220 K), $(LMO)_3/(LAO)_2$ and $(LMO)_4/(LAO)_2$ can be fitted by $R = R_0\exp(E_g/k_BT)$, demonstrating thermally activated behavior［19, 20］, as shown in Fig.4(b). The obtained activation energy E_g are 130 meV, 162 meV and 159 meV for the LMO film, $(LMO)_3/(LAO)_2$ and $(LMO)_4/(LAO)_2$. Obviously, the LAO spacers increase the activation energy, due to its insulating nature.

Conclusion

In summary, we synthesized high-quality fully epitaxial $[(LMO)_t/(LAO)_2]_N$ multilayers (t between 1 and 4 u.c.). The XRD and RSM measurements confirmed the excellent structure and the *c* lattice constant increased with increasing the LMO layer thickness. When $t \geq 2$, the multilayers exhibited ferromagnetic properties and the coercive field reduced with increasing t. All the fabricated multilayers were insulating in nature with much larger activated energy than that of the single layer LMO film. The presented results open an exciting prospect for manipulating the structure, magnetic and transport properties of other LAO-based multilayers (such as $SrRuO_3/LaAlO_3$, $LaNiO_3/LaAlO_3$).

Acknowledgement

Y.K. Liu acknowledges the financial support from the National Natural Science Foundation of China (Grant No.51502129). C.W. Leung acknowledges the financial support from UGC, HKSAR (PolyU 153015/14 P) and PolyU (1-ZE25, 1-ZVGH).

References:

[1] J. Mannhart and D. G. Schlom, Science 327 (2010) 1607.

[2] S. A. Wolf, D. D. Awschalom, R. A. Buhrman, J. M. Daughton, S. von Molnar, M. L. Roukes, A. Y. Chtchelkanova, and D. M. Treger, Science 294 (2001) 1488.

[3] H. Yamada, Y. Ogawa, Y. Ishii, H. Sato, M. Kawasaki, H. Akoh, and Y. Tokura, Science 305 (2004) 646.

[4] M. Imada, A. Fujimori, and Y. Tokura, Rev. Mod. Phys. 70 (1998) 1039.

[5] M. Gibert, P. Zubko, R. Scherwitzl, J. Iniguez, and J. M. Triscone, Nat. Mater. 11 (2012) 1958.

[6] F. Cossu, J. Jilili, and U. Schwingenschlögl, Advanced Materials Interfaces 1 (2014) 1400057.

[7] S. Smadici, P. Abbamonte, A. Bhattacharya, X. Zhai, B. Jiang, A. Rusydi, J. N. Eckstein, S. D. Bader, and J. M. Zuo, Phys. Rev. Lett. 99 (2007) 196404.

[8] J. Chaloupka and G. Khaliullin, Phys. Rev. Lett. 100 (2008) 016404.

[9] A. Biswas, P. B. Rossen, C. H. Yang, W. Siemons, M. H. Jung, I. K. Yang, R. Ramesh, and Y. H. Jeong, Appl. Phys. Lett. 98 (2011) 051904.

[10] X. R. Wang, et al., Science 349 (2015) 716.

[11] A. Gupta, T. R. McGuire, P. R. Duncombe, M. Rupp, J. Z. Sun, W. J. Gallagher, and G. Xiao, Appl. Phys. Lett. 67 (1995) 3494.

[12] W. S. Choi, et al., J. Phys. D: Appl. Phys. 42 (2009) 165401.

[13] A. M. Zhang, S. L. Cheng, J. G. Lin, and X. S. Wu, J. Appl. Phys. 117 (2015) 17B325.

[14] M. Baldini, T. Muramatsu, M. Sherafati, H. K. Mao, L. Malavasi, P. Postorino, S. Satpathy, and V. V. Struzhkin, PNAS 112 (2015) 10869.

[15] Y. S. Hou, H. J. Xiang, and X. G. Gong, Phys. Rev. B 89 (2014)

[16] E. Pavarini and E. Koch, Phys. Rev. Lett. 104 (2010) 086402.

[17] B. R. K. Nanda and S. Satpathy, Phys. Rev. B 81 (2010) 174423.

[18] F. Y. Bruno, et al., Phys. Rev. Lett. 106 (2011) 147205.

[19] S. Middey, D. Meyers, M. Kareev, E. J. Moon, B. A. Gray, X. Liu, J. W. Freeland, and J. Chakhalian, Appl. Phys. Lett. 101 (2012) 261602.

[20] J. Hoffman, I. C. Tung, B. B. Nelson-Cheeseman, M. Liu, J. W. Freeland, and A. Bhattacharya, Phys. Rev. B 88 (2013) 144411.

Figure captions:

Fig.1. An expanded view of the (00*l*) peaks of $(LMO)_t/(LAO)_2$ multilayers, (a) $(LMO)_1/(LAO)_2$, (b) $(LMO)_2/(LAO)_2$, (c) $(LMO)_3/(LAO)_2$, (d) $(LMO)_4/(LAO)_2$.

Fig.2. (a)-(d) X-ray reciprocal space mappings around the (103) peaks for the $(LMO)_t/(LAO)_2$ multilayers. Vertical dashed lines represent the in-plane lattice match to the $SrTiO_3$ substrates.

Fig.3. (a) *M-T* curves of $(LMO)_t/(LAO)_2$ (t=2, 3 and 4) multilayers and single LMO film. (b) Magnetization-filed loops of $(LMO)_t/(LAO)_2$ multilayers at 5 K after field-cooling from room temperature in a +1 T field (blue line) and -1 T field (read line). (c) H_C of $(LMO)_t/(LAO)_2$ at 5 K as a function of thickness of LMO layer and the coercive filed of single-layer LMO.

Fig.4. (a) Sheet resistance for $(LMO)_3/(LAO)_2$, $(LMO)_4/(LAO)_2$ and single-layer LMO as a function of temperature. (b) Resistance-temperature curves plotted in (a) are fitted by thermally activated transport.

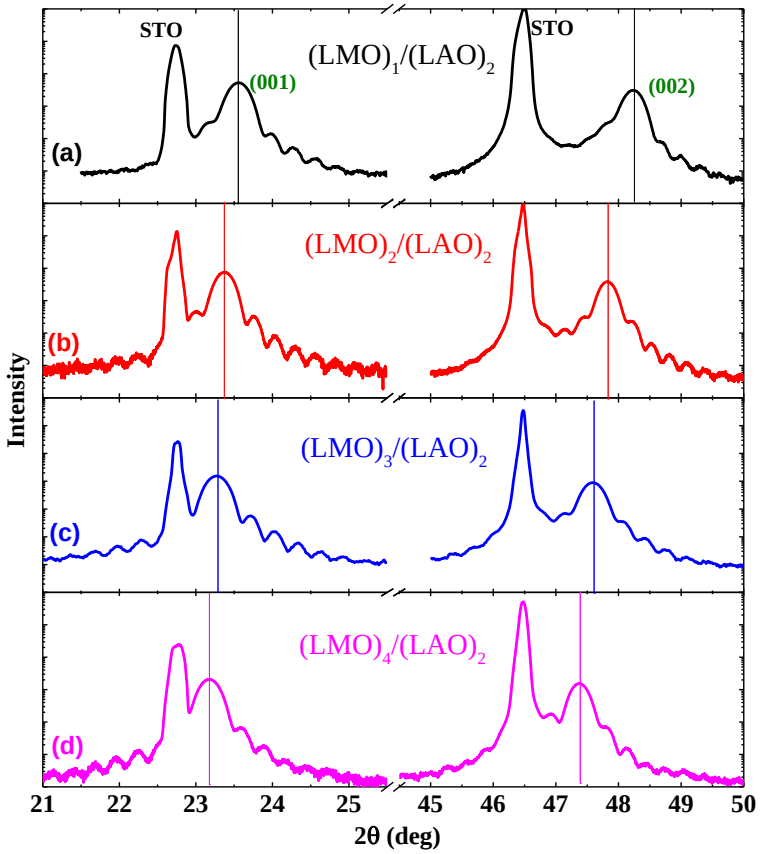
STO
(001)
(LMO)1/(LAO)2
STO
(002)
(a)
(LMO)2/(LAO)2
(b)
(LMO)3/(LAO)2
(c)
(LMO)4/(LAO)2
(d)
Intensity
21
22
23
24
25
45
46
47
48
49
50
2θ (deg)

Fig.1.

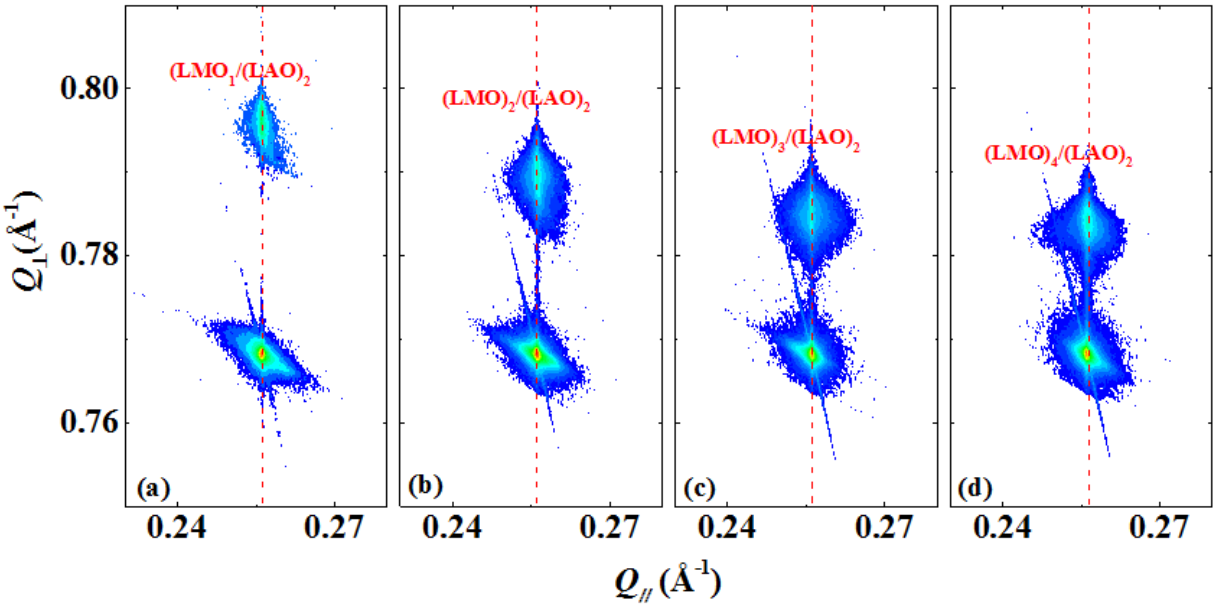
(LMO1/(LAO)2
(LMO)2/(LAO)2
(LMO)3/(LAO)2
(LMO)4/(LAO)2
0.80
0.78
0.76
Q⊥(Å-1)
(a)
(b)
(c)
(d)
0.24
0.27
Q// (Å-1)

Fig.2

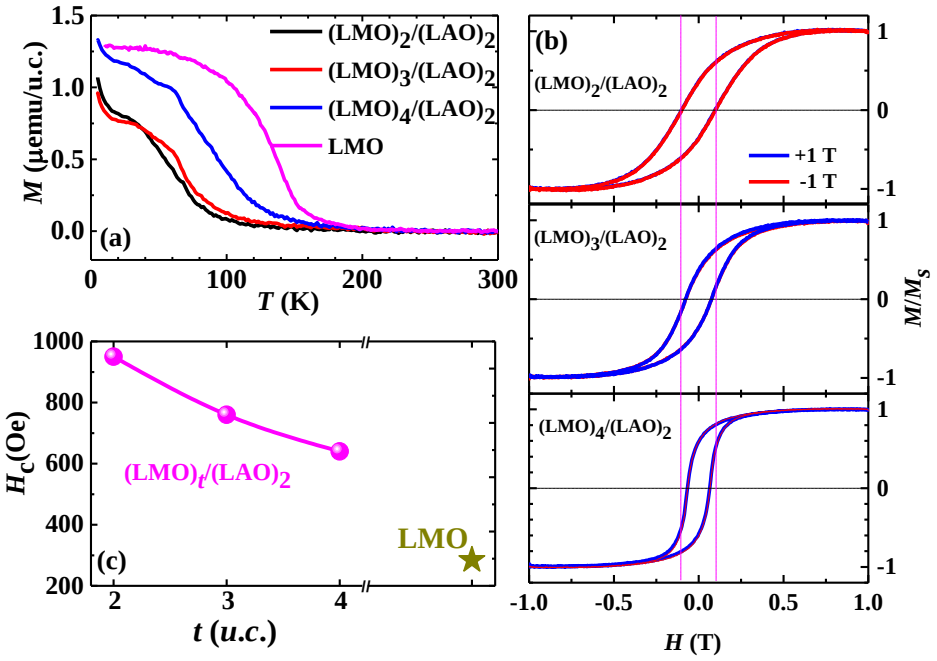
(LMO)2/(LAO)2
(LMO)3/(LAO)2
(LMO)4/(LAO)2
LMO
M (μemu/u.c.)
T (K)
(a)
(b)
+1 T
-1 T
M/MS
H (T)
HC(Oe)
(LMO)t/(LAO)2
LMO
t (u.c.)
(c)

Fig.3

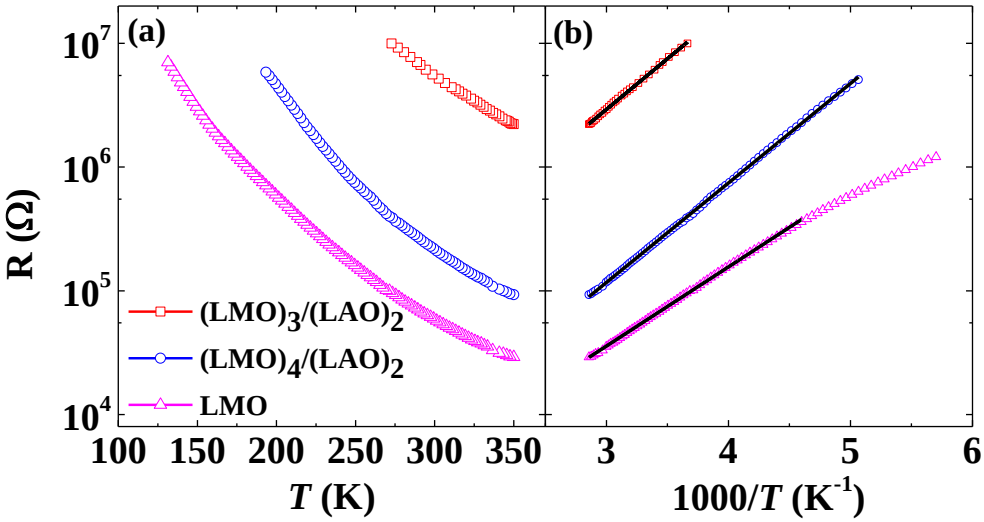
(a)
(b)
R (Ω)
(LMO)3/(LAO)2
(LMO)4/(LAO)2
LMO
T (K)
1000/T (K-1)

Fig.4